Synthesis and optical properties of polythiophene-capped ZnS/Mn quantum dots

Anju Bala[1], Rajeev Sehrawat[1,*] ⓘ, Anil Kumar Sharma[1], and Pardeep Soni[2]

[1] Department of Physics, Maharishi Markandeshwar deemed to be University (MMDU), Mullana, Ambala, Haryana 133207, India
[2] Center of nanotechnology, Indian Institute of Technology Roorkee, Roorkee, Utrakhand 247667, India

ABSTRACT

Polythiophene-capped Mn-doped ZnS (ZnS/Mn) *quantum dots* have been prepared through chemical precipitation method. The characterizations of synthesized *quantum dots* have been performed using X-ray diffraction (XRD), high resolution transmission electron microscope (HRTEM), fourier transform infrared (FT-IR) spectroscopy, UV-visible spectroscopy and photoluminescence (PL) spectroscopy. Particle sizes were nearly 2 nm for both ZnS/Mn and polythiophene (PTh 15%) capped ZnS/Mn samples as estimated using XRD analysis. The estimated particle sizes, after PTh capping on ZnS/Mn, were nearly stable showing that there has been no dilution occurs in the ZnS/Mn *quantum dots* during the synthesis process. The capped ZnS/Mn *quantum dots* show weak agglomeration among them as observed from TEM images, which may be originated due to the electrostatic interaction between the particles as confirmed from the electrostatic potential surface analysis. The particle sizes calculated from the optical absorption spectra were remain consistent with size obtained from TEM images and XRD analysis. It was found that optical absorption bandgap of ZnS nanostructures varies with different concentration of capping agents. This was attributed to the quantum confinement effect. Strong electronic interaction between ZnS and polythiophene was observed from FTIR and electrostatic surface potential analysis which confirms the structural stability of the composite by creating large *dipole moment* of $\sim$ 10.2675 Debye and lagre Mulliken charge $- 0.437486e^-$. The prepared polythiophene-capped samples reveals that the effective PL emission is in the range of 300 nm -700 nm. PL emission spectra show red shift with increasing capping concentration of PTh in ZnS/Mn *quantum dots*. These properties maintained the optical behavior of *quantum dots* and the addition of polymer with ZnS *quantum dots* may improve the flexibility of the nanostructure material, which will be highly preferable for foldable optical devices.

Address correspondence to E-mail: rajeev.sehrawat@gmail.com

1 Introduction

The synthesis of nanostructure materials have proved a beneficial strategy to find the new properties, resulting from the complementarily and synergism between the components. The intense research interest has been gathered by the nanostructured materials owing to the fact of small particle size and large fraction of surface atoms, these materials are expected to exhibit unique size-dependent properties in the research areas such as optical, mechanical, electronic, magnetic, Li-ion and hydrogen storages [1–5]. The size and shape of nanoparticles plays a significant effect on the properties of different applications of nanostructured materials. In the past two decades, various synthesis techniques like solid state reaction, chemical co-precipitation, hydrothermal and sol-gel have been explored to control the morphology and growth of nanoparticles [6–9]. The contribution from the surface energy must be taken into account during the synthesis and application. Surface energy can cause the affects of dilution and agglomeration among nanoparticles and these effects can be suppressed by surface passivation/coatings [10]. The synthesis and desired morphology of nanostructure materials can be obtained using green chemistry based methods, because of low synthesis cost, environmental friendly and better quality of synthesis product.[11, 12] Semiconductor nanomaterials with dimensions ranging between 2 and 20 nm are nanocomposite materials, which have been extensively studied for their interesting size-dependent electrical and optical properties [13, 14]. If their dimensions are smaller than the *exciton* radius of Bohr, *quantum confinement effect* results in the nanoparticles to become *quantum dot*. Among the II-VI compound semiconductor materials, ZnS is a direct-transition semiconductor with the widest energy bandgap (3.67 eV). Because of defects like S vacancies and Zn interstitial, ZnS semiconductor materials have a wide range of applications in luminescence, light-emitting diodes (LEDs), data storage devices, injection lasers. [15]. Accordingly, special attention has been paid to their luminescence properties. Various approaches such as synthesis methods, doping and surface coatings have been adopted by the researchers to improve the photo luminescent properties of ZnS. Different methods of synthesis of ZnS such as spray pyrolysis, hydrothermal [16], electrochemical deposition, sol–gel technique,

chemical co-precipitation and chemical vapor deposition [17] result different morphologies such as nanorods, nanosheets, microspheres and these methods have been studied due to their enhanced optical properties [18]. Among these methods, chemical co-precipitation is easy handling, low temperature and cost effective for the synthesis of ZnS. The photo luminescent properties of ZnS have been improved with doping of atoms with other transition metals like Co, Pb, Cu, Mn. [19]. Doping of these transition metals in the structure of ZnS have been widely studied depending upon the specific research area. Also, it has been desired to dope single element atoms to tune the optical properties of doped ZnS. Doped nanocrystals of ZnS with transition metal atoms are considered to have high quantum efficiency which results improved photo luminescent properties. Among the transition metals, effect of Mn doping in ZnS has been reported by the researchers as it increases the defected sites in the ZnS nanocrystals.

Surface coating of polymers on the ZnS nanoparticles have been extensively studied to improve the optical properties as it reduces the electron hole recombination time and defected sites in the composite. Polymer coated ZnS nanocomposites are usually capped by polyvinylpyrrolidone (PVP), chitosan, 2-mercaptoethanol, Poly (vinyl alcohol) (PVA) and Glutathione, etc. to enhance optical and sensing properties [20–22]. Moreover, polymer based materials show application in foldable display devices and organic light-emitting devices [23]. A suitable capping agent can be identified by the investigation of their effects on the different properties of the nanocomposites. The literature has also reported many examples of nanocomposites having different capping agents over the surface of ZnS nanoparticles. Deka et al. investigates the effect of capping agents on various properties of nanoparticles of ZnS [24], Nguyen et al. studied about the PL properties of the poly(vinyl alcohol)-capped ZnS quantum dots [25], Chen et al. studied about glutathione-capped Mn-doped ZnS *quantum dots* at a room-temperature phosphorescence sensor for the detection of Pb^{2+} ions [26]. Based on these reports, it can be concluded that it is very important to investigate the influence of organic capping agent on the optical properties of ZnS. The polythiophene (PTh), as a conjugated polymer, is considered to be promising candidate for capping owing to its ease of polymerization, efficient

optical property, excellent thermal stability and environmental friendly. PTh also shows absorption and emission spectra in the visible region [27]. Although, preparation of capped ZnS nanocomposites have been adopted by researchers worldwide for achieving the structural and optical properties, but PTh coating on Mn-doped ZnS has not been reported in the literature. We have used chemical co-precipitation method for synthesis of Mn-doped ZnS and oxidative polymerization for the synthesis of long chain PTh molecules from their monomers to investigate the structural and optical properties.

2 Experimental analysis

2.1 Materials

Zinc acetate ($ZnC_4H_6O_4$) AR (99.5%), manganese acetate tetra hydrate ($C_4H_6M_gO_4.4H_2O$) GR (99.5%) and sodium sulfide (Na_2S) GR (99.9%) were obtained from Loba chemie., thiophene (C_4H_4S) GR (99%), ferric chloride anhydrous ($FeCl_3$) GR (97%), dichloromethane (CH_2Cl_2) GR(99.8%), ethanol (C_2H_5OH) GR (99.8%) and acetonitrile (CH_3CN) GR (99.8%) were purchased from Sigma-Aldrich.

2.2 Methods

2.2.1 Synthesis of manganese doped ZnS (ZnS/Mn)

Mn-doped ZnS *quantum dots* were synthesized by chemical co-precipitation method. The powder forms of zinc acetate, manganese acetate and sodium sulphide were used as source for Zn, Mn and S, respectively. A solution of 0.6373 g of manganese acetate in 20ml distilled water solvent was added drop wise to another solution containing 11.19 g zinc acetate in solvent of 50ml deionized water. For the growth of Mn-doped ZnS, 3.98 g of sodium sulphide was mixed in 50 ml distilled water and drop wise added to the above solution followed by stirring for half an hour. This leads to the formation of white precipitates of ZnS/Mn, which was further centrifuged and washed many times with distilled water and ethanol. The powder was dried in vacuum for 12 h at 60 °C, followed by the de-agglomeration of the particles using pestle-mortar to get a fine powder.

2.2.2 Synthesis of polythiophene

Polythiophene was synthesized by oxidative polymerization method using $FeCl_3$ as an oxidizing agent. For the polymerization, 85 ml thiophene monomers were drop wise added to 100 ml dichloromethane to make the precursor solution. In another beaker, oxidizing solution was prepared by dissolving 17.32 g of $FeCl_3$ in 50 ml of acetonitrile solvent and stirred for 30 min. The oxidizing solution was added drop wise to the precursor and immediate formation of black precipitates confirm the beginning of polymerization of monomer units. The stirring was allowed to continue for 24 h till all the monomer units form polymer. Precipitates were filtered and properly washed with acetone to flush the extra ions. The wet material, black in color, was obtained which was further dried in vacuum at 60 °C for overnight to get the polythiophene.

2.2.3 Synthesis of PTh coated ZnS/Mn (PTh-ZnS/Mn) quantum dots

Synthesis of the PTh capped ZnS/Mn *quantum dots* was carried out by in situ polymerization method as shown in Fig. 1. 2 g of Mn-doped ZnS powder was wetted with thiophene monomer for 10 min. Then, 50 ml CH_3Cl_2 was added to the above solution with continuous stirring for 30 min. $FeCl_3$, as oxidizing agent, was dissolved in 50 ml acetonitrile with a mole ratio of $FeCl_3$ to thiophene as (1:3). After that, this solution was added drop wise to above solution to initiate polymerization. The solution was kept on stirring for 24 h. After that, solution was filtered and the black residue was washed with acetone followed by drying under vacuum at 60 °C for overnight. The black residue was further de-agglomerated using mortal-pestle to get the final composite in fine powder form. In this way, 6, 9, 12 and 15 wt% of PTh capped ZnS/Mn composite materials were synthesized as PTh (6%)-ZnS/Mn, PTh (9%)-ZnS/Mn, PTh (12%)-ZnS/Mn and PTh (15%)-ZnS/Mn samples.

2.3 Characterizations

X-ray diffraction (XRD) patterns were taken on powder X-ray diffractometer (PANalytical X'Pert Pro) using Cuk_α radiation (λ = 1.5406 Å) at scanning rate of 1.5 degree/min with step size 0.0188 degree to
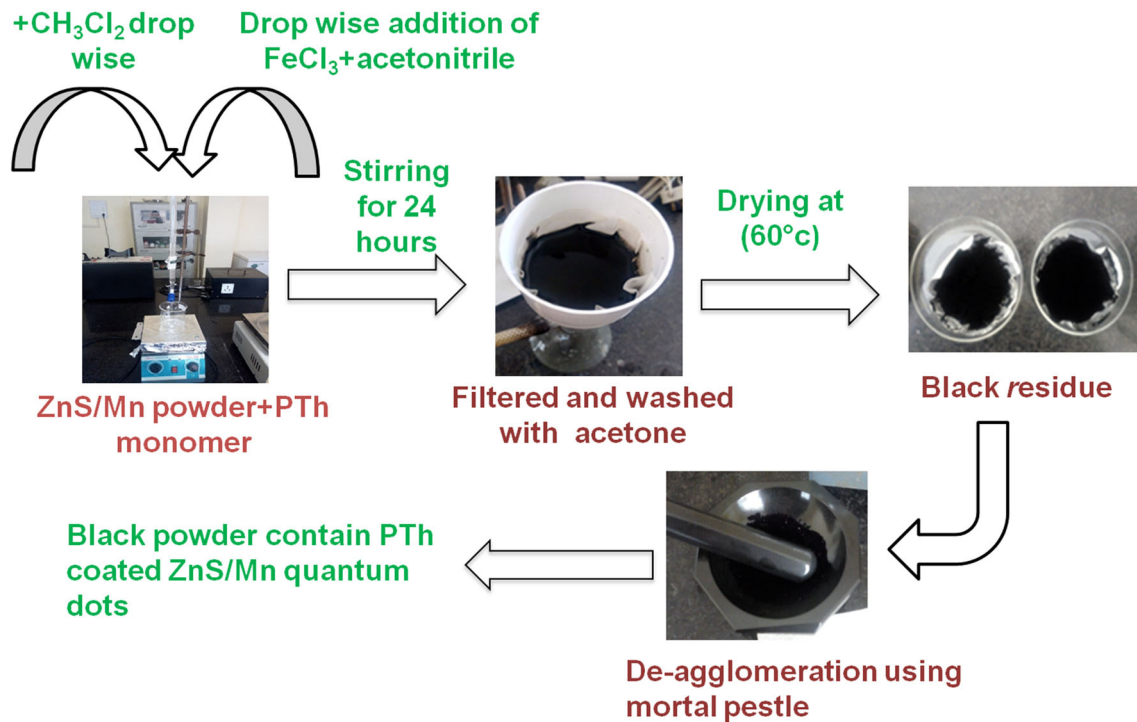
Fig. 1 Schematic diagram of PTh capped ZnS/Mn quantum dots

identify the crystal structure of the samples. After this, phase analysis of the samples was performed using X-ray diffraction software (PANalytical X'Pert HighScore Plus 2.2.0). High resolution transmission electron microscope (HRTEM) (TECNAI G20 HR-TEM) at 200 kV was used to examine the morphology of the particles. Perkin Elmer (Spectrum RX-I) was used to study the Fourier transform infrared (FT-IR) vibrational spectra of the samples. The absorption spectra and PL spectra of all the samples were recorded at a concentration of 10 mg/ml (using ethanol solvent) in the range of 300 nm to 700 nm with step-size of 2 nm on Multi-mode Microplate Reader (Synergy H1) hybrid from BioTek. Electrostatic potential surface analysis of the samples was performed using Ab-initio computation using G-03 and Gauss View 4.1 computed by DFT(B3LYP)6-31G method in the Department of Physics, MMEC, MMDU.
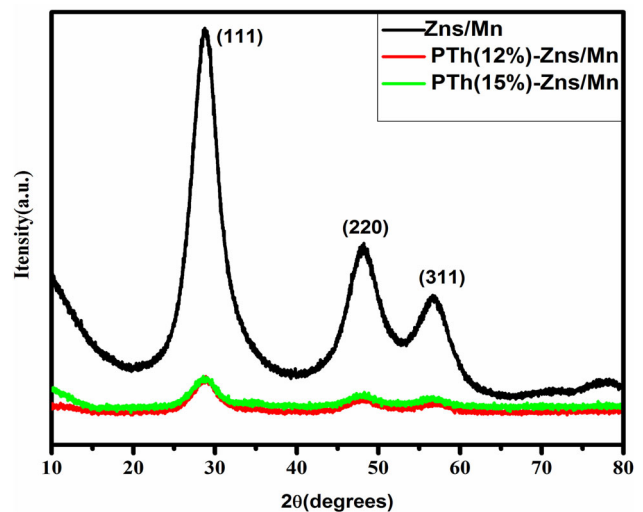

Fig. 2 XRD pattern of ZnS/Mn and PTh-capped ZnS/Mn quantum dots

3 Results and discussion

3.1 X-ray diffraction (XRD) study

Figure 2 shows the XRD patterns of ZnS/Mn and PTh-ZnS/Mn samples. For ZnS/Mn *quantum dots*, the major diffraction peaks were observed at $2\theta = 28.74°$, $48.06°$ and $56.64°$ corresponding to (111), (220) and

(311) planes of cubic zinc–blend structure respectively and the structure matched with the standard card (JCPDS-No.01-080-0020) belongs to the space group F-43 m (space group no. 216). PTh-ZnS/Mn nanocomposites show well-defined peaks with no shift in the peak position as compared to the ZnS/Mn quantum dots which reflects that there was no change in the inter planar spacing in the crystal structure of ZnS. However, decrease in peak intensities reflects the formation of PTh capping in the composite structure. The average particle sizes of ZnS/Mn and PTh-ZnS/Mn samples were estimated using Scherrer's Eq. (1) [28].

$$D = \frac{K\lambda}{\beta \mathrm{Cos}\theta} \tag{1}$$

where D is the average particle size, $K = 0.9$, λ is the wavelength of CuK_α radiation (1.54 Å), θ is the *Bragg angle* and β is the full width at half maxima of highest peak intensity at 28.74. The estimated size was 2 nm for both the samples of ZnS/Mn, PTh(12%)-ZnS/Mn and PTh(15%)-ZnS/Mn. This is fairly in the range of *exciton* Bohr's radius for ZnS (which is 2.5 nm), hence strong quantum confinement effects can be expected in the optical properties of these samples. The particle size of ZnS/Mn before and after the capping is nearly stable showing that there is no dilution of particles during the polymerization of thiophene monomers.

3.2 Morphological studies

Detailed morphological study has been carried out using HRTEM to further investigate the polymer capping on ZnS. The TEM image in Fig. 3(a) revealed nearly spherical and well dispersed ZnS/Mn particles. Particle size analysis was performed using 'imageJ' software and the size distribution of *quantum dots* was fitted with Gaussian curve shown in Fig. 3(d) The Gauss fitting of size distribution was ranged from 1.5 to 4.5 nm with an average size of 2.75 nm which was very close to *exciton* Bohr radius of ZnS. The full-width-at-half-maximum (FWHM) of the Gaussian curve was 1.17 nm. Figure 3(b) and 3(c) show TEM image of PTh-ZnS/Mn nanocomposite at different magnifications. From the TEM images, it was clearly observed that capped ZnS *quantum dots* were agglomerated; this was due to strong electronic interaction of polymer chains with the ZnS/Mn *quantum dots*. The size of most of the PTh-ZnS/Mn particles was in the range of 2 to 3 nm,

which was well in agreement with the size obtained from XRD analysis.

3.3 Fourier transform infrared (FTIR) spectroscopy

FTIR spectra of synthesized samples of pure PTh and PTh-ZnS/Mn nanocomposites have been shown in Fig. 4.The FTIR graph has displayed the major characteristics peaks of nanocomposites in finger print region (500–4000 cm^{-1}). In the FTIR spectra of pure PTh (Fig. 4), peaks were located at 673.5 cm^{-1}, 791.5 cm^{-1},1036.0 cm^{-1}, 1114.0 cm^{-1}, 1331.26 cm^{-1}, 1639.06 cm^{-1} and 3430.0 cm^{-1} which revealed the main characteristics peaks of pure PTh. In the details, a broad peak located at nearly 3430 cm^{-1} was attributed to O-H stretching vibration of water molecules [29]. The appearance of peak at 1639.06 cm^{-1} corresponds to C=C symmetric stretching vibrations of the thiophene ring [30]. The small and weak peaks at 673.5 cm^{-1}, 791.5 cm^{-1} were attributed to C–S thiophene stretching and C–H out-of-plane vibrations [31]. On the other hand, two well sharp peaks situated at 1036.0 cm^{-1}and 1331.26 cm^{-1} assigned to the C-H plane deformation mode and C-H stretching vibration, respectively [32]. Another peak situated at 1114.0 cm^{-1} belongs to C–H bending vibration. The spectra of PTh-ZnS/Mn nanocomposites peaks were shifted slightly as compare to pure PTh. The peaks at 3430.0 cm^{-1}, 1639.6 cm^{-1}, 1036.0 cm^{-1}, 673.50 cm^{-1} were shifted to 3394.9 cm^{-1}, 1621.1 cm^{-1}, 1019.3 cm^{-1}, 689.9 cm^{-1} respectively for PTh-ZnS/Mn nanocomposites. The strong peak was observed at 689.9 cm^{-1} due to the Zn-S stretching vibrations which may be originated from the combined effect of bond formed between S of polymer and Zn of ZnS, and C–S thiophene stretching [33]. Also, in the case of PTh-ZnS/Mn nanocomposites, an additional peak was observed at 1423.9 cm^{-1} which may be related to –OH deformation vibration of tertiary C–OH stretching vibration. The moisture present in the sample was confirmed by appearance of broad band at 3854.8 cm^{-1}, which corresponds to O-H stretching vibration. Slight peak shifting for PTh-ZnS(Mn) composite material may arise due to the interaction between ZnS and PTh.
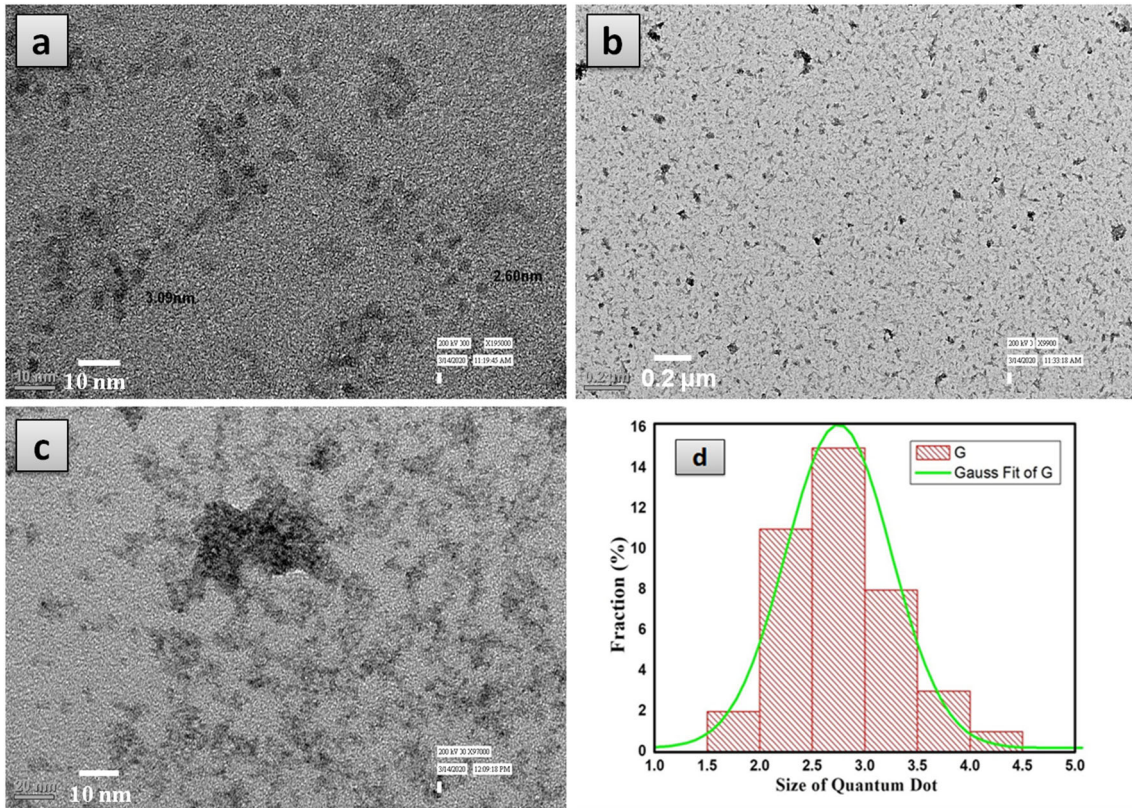
Fig. 3 a HR-TEM image of ZnS/Mn *quantum dots*. **b** PTh-ZnS/Mn *quantum dots* at low magnification **c** PTh-ZnS/Mn *quantum dots* at high magnification. **d** Gaussian curve of ZnS/Mn *quantum dots*
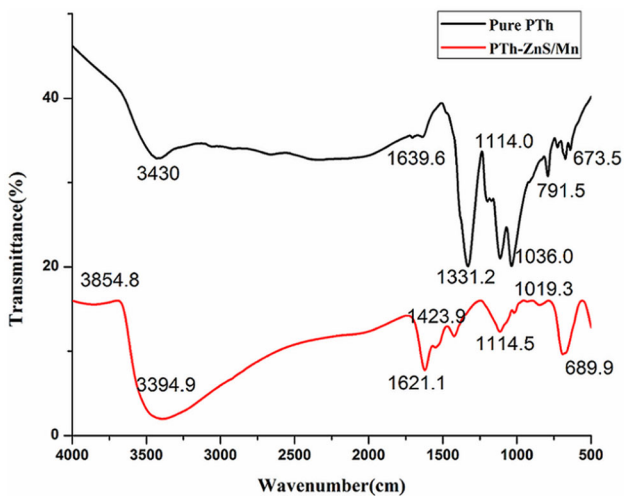

Fig. 4 FTIR spectra of Pure PTh and PTh-ZnS/Mn nanocomposites

3.4 UV–Vis spectroscopic and Tauc's plot

UV-vis absorption spectroscopy is an efficient method to monitor the inverse relationship between optical properties and particle size of material. The absorption peaks were observed at 295 nm, 305 nm, 310 nm, 300 nm, and 315 nm wavelengths for ZnS/Mn, PTh (6%, 9%, 12 and 15%) capped ZnS/Mn *quantum dots* respectively are shown in Fig. 5a. The direct energy bandgap of all the samples was determined from UV-visible spectral data using Tauc's Eq. (2):

$$(\alpha h \upsilon)^2 = A(h \upsilon - E_g) \tag{2}$$

(where α, h, υ, A and E_g is the absorption coefficient, Planck's constant, photon's frequency, proportionality constant and optical bandgap energy, respectively) [34]. Bandgap energy for all the samples were calculated by measuring the x-intercept obtained from extrapolating the fitting of linear region of $(\alpha h \upsilon)^2$ versus $h\upsilon$ [35] graph of above equation. The energy bandgaps calculated from Fig. 5(b) for ZnS/Mn, PTh(6%)-ZnS/Mn, PTh(9%)-ZnS/Mn, PTh(12%)-ZnS/Mn and PTh(15%)ZnS/Mn samples were 4.21, 4.02, 4.07, 4.14 and 3.92 eV, respectively. From the absorption spectra of all the samples, it was found that PTh (12) % capped ZnS/Mn nanocomposite has maximum bandgap, i.e. 4.14 eV, which shows better
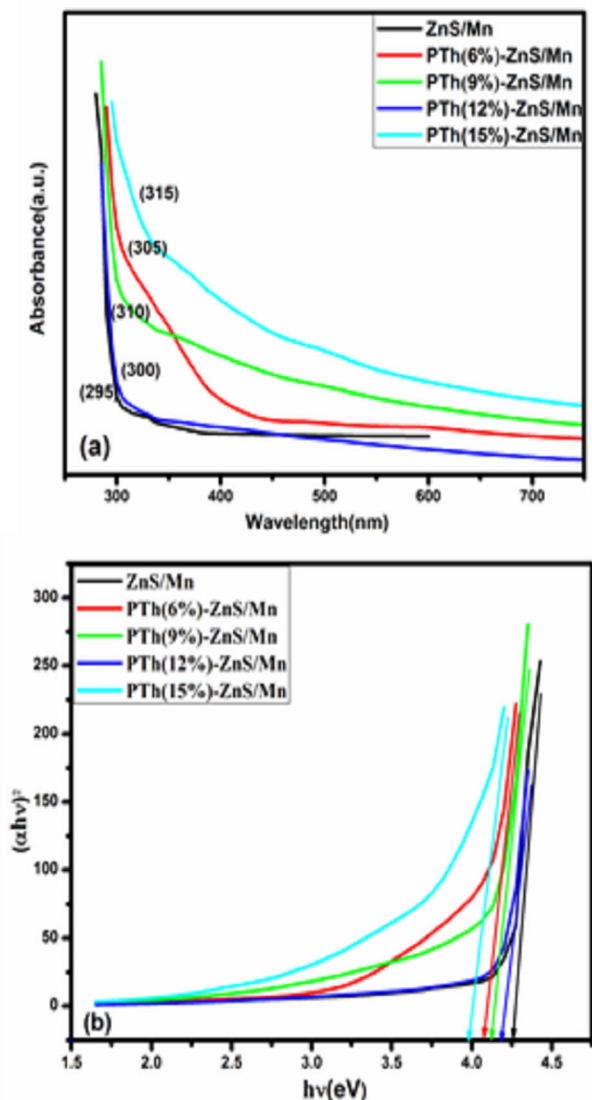
Fig. 5 a Optical absorption spectra and **b** Tauc's plot of ZnS/Mn and PTh- ZnS/Mn nanocomposites

quantum confinement effect compared to another capped samples, while strong *quantum confinement effect* was observed in all the capped and uncapped ZnS/Mn samples in comparison to the bulk ZnS which has a bandgap of 3.68 eV. From the position of absorption edge, the average particle size (2R) of the *quantum dots* can be determined by empirical formula Eq. (3):

$$2R = 0.1 nm/(0.138 - 0.0002345\lambda_c) \qquad (3)$$

where *2R* is diameter of particle and λ_c is the absorption edge [36]. The absorption edge (λ_c) can be determined by the intersection of sharply decreasing region of spectrum with the baseline. The average particle size of 1.45 nm was calculated for ZnS/Mn

quantum dots with λ_c at 295 nm, while it was 1.50 nm, 1.53 nm, 1.47 nm and 1.55 nm for PTh(6%)-ZnS/Mn, PTh(9%)-ZnS/Mn, PTh(12%)-ZnS/Mn and PTh(15%)-ZnS/Mn samples measured using λ_c as 305 nm, 310 nm, 300 nm and 315 nm, respectively. A small increment in particle diameter was observed with the addition of weight percents of PTh in the PTh-ZnS/Mn samples. This increment may be due to the capping of PTh layer on the ZnS/Mn quantum dots. The evaluated particle sizes of all the samples were below the limit of *exciton* Bohr's radius (which is 2.5 nm), so the synthesized nanoparticles can be treated as quantum dots. Increased value of diameter indicates the larger size of polythiophene-capped ZnS/Mn nanocomposites, which was already verified by XRD analysis.

3.5 Photoluminescence (PL) study

PL emission spectra in the wavelength range of 300 nm to 700 nm of ZnS/Mn and PTh-ZnS/Mn samples are shown in Fig. 6 which gives similar trends as in absorption spectra. The emission spectrum of ZnS/Mn *quantum dots* shows peak intensities at 309 nm and 603 nm under UV and orange wavelength range, respectively. Wavelength of emission peak at 309 nm had been attributed to the recombination process associated with sulphur vacancies in the ZnS/Mn *quantum dots* [37]. A set of emission peaks corresponding to 309 nm of ZnS/Mn was observed for PTh-ZnS/Mn samples between 309 nm to 313 nm,
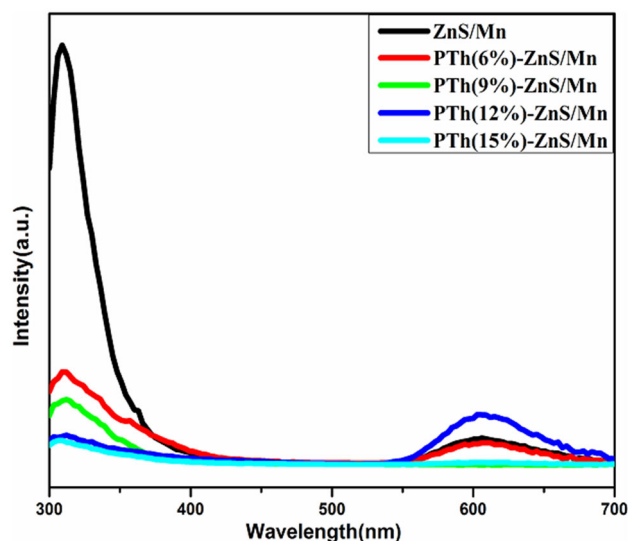

Fig. 6 PL emission spectra of ZnS/Mn and PTh capped ZnS/Mn *quantum dots*

where Fig. 6 shows that, with PTh capping on ZnS, these emission peaks are shifted slightly to higher wavelength region causing the red shift. The wavelength of emission peak at 603 nm was also observed for ZnS/Mn sample which corresponds to the orange region of the visible spectrum. This peak arises due to 4T1-6A1 transition of Mn. A set of peaks corresponding to 4T1-6A1 transition of Mn were also observed at 603.5 nm, 605 nm, 605.9 nm and 606.7 nm for PTh(6%)-ZnS/Mn, PTh(9%)-ZnS/Mn, PTh(12%)-ZnS/Mn and PTh(15%)-ZnS/Mn samples, respectively. Red shift was observed for both the sets of peaks in PTh-ZnS/Mn samples when compared with uncapped ZnS/Mn quantum dots. The observed red shift signifies the marginal increment in size of *quantum dots* with increment of weight% of capping agent which is inconsistent with the UV-vis results. The PL results are in agreement with the UV results which show that ZnS *quantum dots* maintained their optical properties even after capping with PTh.

3.6 Theoretically calculations

Ab-initio computation of electrostatic potential surface analysis of PTh (of three thiohene monomer units) using DFT (B3LYP)6-31G method were computed by G-03 and Gauss View 4.1 in the Department of Physics, MMEC, MMDU. From electrostatic potential surface analysis of PTh, it was found that ZnS get attached with thiophene monomer as shown in Fig. 7a. It was also found that H_7, H_8, H_{13}, H_{15}, H_{20} and H_{22} shown in Fig. 7b are more electropositive sites as compared to others; hence these sites have higher possibilities of being attacked by electronegative species. On the other hand, electronegative sites of PTh, as shown in Fig. 7c, are found at S_5, S_{11} and S_{18} positions, hence these sites have higher possibilities to be attacked by electro-positive species. It can be concluded that for PTh-ZnS/Mn composite material, Zn has greater affinity to get attracted toward the S_5, S_{11} and S_{18} sites of PTh. So, the interaction between ZnS/Mn and PTh chains is energetically favorable for the bond formation which leads to the greater stability of the PTh polymer chains. Further, the potential surface analysis of the PTh-ZnS/Mn composite material, as shown in Fig. 7d, confirms the interaction between PTh and ZnS, which occurs through Zn and S_5, S_{11} and S_{18} sites of PTh. At the same time, the bond lengths between S_5-Zn_{24}, S_{11}-

Zn_{28}, S_{18}-Zn_{26} have been increased and Zn_{24}-S_{25}, Zn_{28}-S_{29}, Zn_{26}-S_{27} have been decreased (shown in Table 1) when compared to bulk ZnS (2.36). Larger bond length indicates the structural distortion of ZnS and PTh that generates defective sites on these molecules, which results the optical properties in PTh-ZnS/Mn quantum dots. Also, the interaction between ZnS and PTh creates a large negative Mulliken charge of -0.437486 e⁻ on the free end of ZnS making this end strongly electronegative, as shown in Fig. 7d, due to which this site has higher affinity to attract the electropositive site of the nearby PTh chains covering the ZnS.

Dipole moments of PTh and PTh-ZnS/Mn composites were calculated as 0.9534 and 10.2675 Debye using DFT (B3LYP)6-31G method, respectively. The higher *dipole moment* of PTh-ZnS/Mn reflects the higher asymmetry of the molecule as compared to PTh, due to which composite material has more surface charges. Large dipole moments create strong interaction among them; due to this PTh-ZnS/Mn composite particles may interact strongly. The TEM images also confirmed the agglomeration among the particles arise from the strong interaction from these dipoles.

4 Conclusions

Chemical precipitation method was used for the synthesis of ZnS/Mn particles and further oxidation polymerization process was performed to cap these particles by PTh. The XRD studies confirm the formation of Mn-doped cubic zinc–blend structure of ZnS in both ZnS/Mn and PTh-ZnS/Mn samples with particles size nearly 2 nm. The particle size before and after capping is nearly stable and close to the *exciton* Bohr radius (which is 2.6 nm for ZnS) reflecting the *quantum confinement effect* for bare ZnS/Mn and PTh-ZnS/Mn samples. TEM images show the agglomeration for PTh capped ZnS/Mn quantum dots, this is due to the strong electronic interaction caused by the *dipole moment* of ~ 10.2675 Debye, generated by the polymer chains on ZnS/Mn *quantum dots* as calculated by the electrostatic potential surface analysis. ZnS interacts with the PTh chains which makes free end of ZnS as strong electronegative with Mulliken charge of -0.437486 e⁻ creating
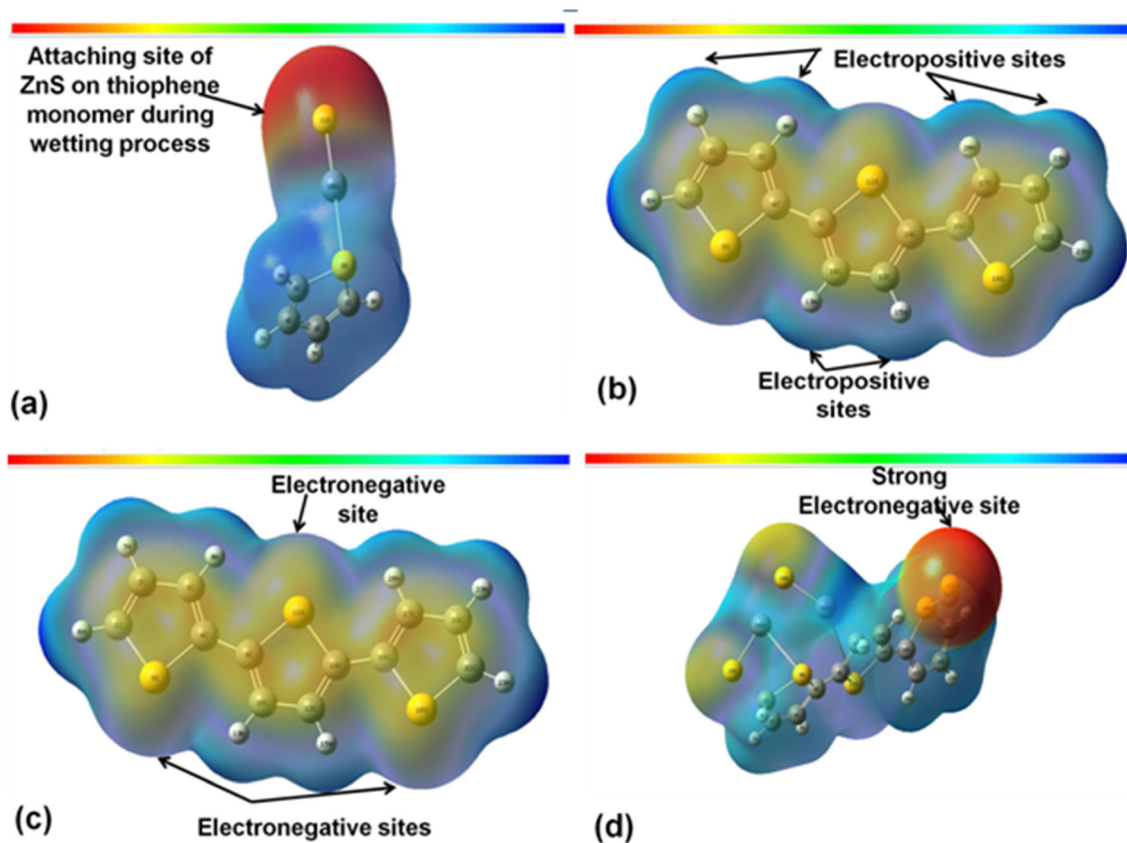
Fig. 7 Optimized geometry of **a** ZnS attach with thiophene monomer, **b** electro positive site of pure polythiophene **c** electro negative site of pure polythiophene. **d** ZnS attach with polythiophene

Table 1 Comparison between Zn and S bond lengths for PTh-ZnS/Mn composites

Molecules	Bond length between Zn and S of PTh (Å)	Bond length between Zn and S of ZnS (Å)
S_5-Zn_{24}-S_{25}	2.8	2.25
S_{11}-Zn_{28}-S_{29}	3.9	2.2
S_{18}-Zn_{26}-S_{27}	2.4	2.08

this end more susceptible to electropositive sites of other polymer chains. So, the large *dipole moment* and higher Mulliken charge confirm that the bond formation between ZnS and polymer is energetically favorable because of presence of electronegative sites on the polythiophene chains. UV-vis spectroscopy confirmed the *quantum confinement effect* for the polythiophene-capped ZnS/Mn composite. The PL spectra of all samples confirmed two sets of emission peaks corresponding to 309 and 603 nm. The emission spectra corresponding to 309 nm is due to sulphur vacancy where another set at 603 nm originates due to $4T_1$-$6A_1$ transition in Mn. The minor particle size increment results in marginal red shift PL spectra of ZnS/Mn particles after PTh capping. The PTh-ZnS/Mn nanostructure material have shown appreciable optical properties, where the addition of polymer to ZnS *quantum dots* may improve the flexibility of the nanostructure material which can be used for the foldable displays and organic light-emitting diodes applications [38].

References

1. M.S. Morassaei, S.Z. .Ajabshir, M. S.Niasari, Adv. Powder Technol. **28**(3), 697–705 (2017)

2. X. Xu, D. Zhang, Z. Wang, S. Zuo, J. Yuan, R. Hu, J. Liu, ACS Appl. Mater. Interfaces **13**(9), 11007–11017 (2021)

3. R. Kumar, P. Sakthivel, P. Mani, Optik **240**, 166788–166809 (2021)

4. R. Sehrawat, A. Sil, J. Mater. Sci.: Mater. Electron. **26**(7), 5175–5185 (2015)

5. S. Z.Ajabshir, M.S. Morassaei, O. Amiri, M.S. Niasari, L.K. Foong, Ceram. Int. **46**(11), 17186–17196 (2020)

6. S.Z. Ajabshir, M. Baladi, M.S. Niasari, Ultrason. Sonochem. **72**, 105420 (2021)

7. S.Z. Ajabshir, Z. Salehi, M.S. Niasari, J. Clean. Prod. **192**, 678–687 (2018)

8. S. Ashrafi, M.M. Kamazani, S.Z. .Ajabshir, A. Asghari, Int. J. Hydrogen Energy **45**(41), 21611–21624 (2020)

9. S. Z.Ajabshir, M. M.Kamazani, Ceram. Int. **46**(17), 26548–26556 (2020)

10. S.Z. Ajabshir, N. Ghasemian, M.M. Kamazani, M. S.Niasari, Ultrason. Sonochem. **71**, 105376 (2021)

11. S.Z. Ajabshir, N. Ghasemian, M. S.Niasari, Ceram. Int. **46**(1), 66–73 (2020)

12. S.Z. Ajabshir, M.S. Morassaei, O. Amiri, M.S. Niasari, Ceram. Int. **46**(5), 6095–6107 (2020)

13. W. Shuang, A. Li, D.H. Wang, Z. Chang, J. Solid State Chem. **276**, 159–163 (2019)

14. R.N. Bhargava, D. Gallagher, X. Hong, A. Nurmikko, Phys. Rev. Lett. **72**, 416–419 (1994)

15. V. Lahariya, M. Ramrakhiani, Luminescence **35**(6), 924–933 (2020)

16. M. Kuppayee, G.V. Nachiyar, V. Ramasamy, Appl. Surf. Sci. **257**(15), 6779–6786 (2011)

17. S. Muruganandam, G. Murugadoss, Optik **220**, 165187 (2020)

18. G. Lee, J.J. Wu, Powder Technol. **318**, 8–22 (2017)

19. A. Divya, B.K. Reddy, S. Sambasivam, K.S. Kumar, P.S. Reddy, Physica E **44**(3), 541–545 (2011)

20. J. Osuntokun, P.A. Ajibade, Journal of Nanomaterials **2016**, 1–14 (2016)

21. H.R. Rajabi, M. Farsi, Mater. Sci. Semicond. Process. **48**, 14–22 (2016)

22. Z. Bujnakova, E. Dutkova, M. Kello, J. Mojzis, M. Balaz, P. Balaz, O. Shpotyuk, Nanoscale Res. Lett. **12**(328), 1–9 (2017)

23. M.C. Choi, Y. Kim, C.S. Ha, Prog. Polym. Sci. **33**(6), 581–630 (2008)

24. D.C. Deka, A. Kalita, S. Bardaloi, M.P. Kalita, J. Lumin. **210**, 269–275 (2019)

25. T.P. Nguyen, Q.V. Lam, T.B. Vu, J. Lumin. **203**, 533–539 (2018)

26. J. Chen, Y. Zhu, Y. Zhang, Spectrochim. Acta Part A Mol. Biomol. Spectrosc. **164**, 98–102 (2016)

27. A.O. Patil, A.J. Heeger, F. Wudl, Chem. Rev. **88**(1), 183–200 (1988)

28. R.K. Chandrakar, R.N. Baghel, V.K. Chandra, B.P. Chandra, Superlatt. Microstruct. **86**, 256–269 (2015)

29. R. Kalyani, K. Gurunathan, Optik **127**(11), 4741–4745 (2016)

30. E.S. J.Zia, U. Aazam, Riaz, J. Mol. Struct. **1207**, 127790 (2020)

31. J.Chen,L. Zhang, J. Zhu, N. Wang, J. Feng, W. Yan, Appl. Surf. Sci. **459**, 318–326 (2018)

32. M. Faisal, F.A. Harraz, A.A. Ismail, A.M. El-Toni, S.A. Al-Sayari, A. Al-Hajry, M.S. Al-Assiri, Sep. Purif. Technol. **190**, 33–44 (2018)

33. K.K. Rasu, P. Sakthivel, G.P. Venkatesan, Opt. Laser Technol. **130**, 106365 (2020)

34. P.A. Ajibade, A.E. Oluwalana, B.M. Sikakane, M. Singh, Chem. Phys. Lett. **755**, 137813 (2020)

35. S.M. Morassaei, S.Z. Ajabshir, M.S. Niasari, J. Mater. Sci.: Mater. Electron. **27**(11), 11698–11706 (2016)

36. M. Rana, P. Chowdhury, J. Lumin. **206**, 105–112 (2019)

37. H.C. Warad, S.C. Ghosh, B. Hemtanon, C. Thanachayanont, J. Dutta, Sci. Technol. Adv. Mater. **6**(3–4), 296–301 (2005)

38. S.R. Jayasudha, K.V. Sreeja, L. Priya, K.T. Vasudevan, Arch. Appl. Sci. Res. **8**(3), 38–45 (2016)